

## MIT Open Access Articles

*Quantifying Cell-to-Cell Variation in Power-Law Rheology*

The MIT Faculty has made this article openly available. **Please share** how this access benefits you. Your story matters.

**Citation:** Cai, PingGen, Yusuke Mizutani, Masahiro Tsuchiya, John M. Maloney, Ben Fabry, Krystyn J. Van Vliet, and Takaharu Okajima. "Quantifying Cell-to-Cell Variation in Power-Law Rheology." *Biophysical Journal* 105, no. 5 (September 2013): 1093–1102. © 2013 Biophysical Society

**As Published:** <http://dx.doi.org/10.1016/j.bpj.2013.07.035>

**Publisher:** Elsevier

**Persistent URL:** <http://hdl.handle.net/1721.1/92372>

**Version:** Final published version: final published article, as it appeared in a journal, conference proceedings, or other formally published context

**Terms of Use:** Article is made available in accordance with the publisher's policy and may be subject to US copyright law. Please refer to the publisher's site for terms of use.



# Quantifying Cell-to-Cell Variation in Power-Law Rheology

PingGen Cai,<sup>†</sup> Yusuke Mizutani,<sup>†</sup> Masahiro Tsuchiya,<sup>†</sup> John M. Maloney,<sup>‡</sup> Ben Fabry,<sup>§</sup> Krystyn J. Van Vliet,<sup>‡¶</sup> and Takaharu Okajima<sup>†\*</sup>

<sup>†</sup>Graduate School of Information Science and Technology, Hokkaido University, Sapporo, Japan; <sup>‡</sup>Department of Materials Science and Engineering, Massachusetts Institute of Technology, Cambridge, Massachusetts; <sup>§</sup>Department of Physics, The University of Erlangen-Nuremberg, Erlangen, Germany; and <sup>¶</sup>Department of Biological Engineering, Massachusetts Institute of Technology, Cambridge, Massachusetts

**ABSTRACT** Among individual cells of the same source and type, the complex shear modulus  $G^*$  exhibits a large log-normal distribution that is the result of spatial, temporal, and intrinsic variations. Such large distributions complicate the statistical evaluation of pharmacological treatments and the comparison of different cell states. However, little is known about the characteristic features of cell-to-cell variation. In this study, we investigated how this variation depends on the spatial location within the cell and on the actin filament cytoskeleton, the organization of which strongly influences cell mechanics. By mechanically probing fibroblasts arranged on a microarray, via atomic force microscopy, we observed that the standard deviation  $\sigma$  of  $G^*$  was significantly reduced among cells in which actin filaments were depolymerized. The parameter  $\sigma$  also exhibited a subcellular spatial dependence. Based on our findings regarding the frequency dependence of  $\sigma$  of the storage modulus  $G'$ , we proposed two types of cell-to-cell variation in  $G'$  that arise from the purely elastic and the frequency-dependent components in terms of the soft glassy rheology model of cell deformability. We concluded that the latter inherent cell-to-cell variation can be reduced greatly by disrupting actin networks, by probing at locations within the cell nucleus boundaries distant from the cell center, and by measuring at high loading frequencies.

## INTRODUCTION

The living cell is a compliant, viscoelastic material with a highly dynamic and continuously remodeling cytoskeleton (CSK) (1–4). The rheological properties of adherent cells are mainly attributed to the CSK and are related to various cell functions (5–9). Studies have revealed that rheological parameters as the creep compliance and the complex shear modulus,  $G^*$ , which were measured at arbitrarily positions of cells and/or spatially averaged, follow single (10–24) or multiple (25–29) power-law behaviors over multiple decades around 10 Hz.

On the other hand, the inherently heterogeneous CSK structure results in spatial variation in cell elasticity (30,31) and rheology (32) measurements. Recently, Park et al. (33) investigated the local heterogeneity of the ensemble-averaged shear modulus by measuring a large number of single cells that were cultured on micropatterned substrates. Using a single power-law rheology model (15,16,34), they showed that in addition to the stiffness, the power-law exponent and the Newtonian viscosity also depend on the choice of subcellular region probed (33). Moreover, previous studies have revealed universal features of cell-to-cell mechanical variation: the number (ensemble) distribution of  $G^*$  exhibits a log-normal distribution, whereas the power-law exponent exhibits a normal, or Gaussian, distribution (23–26,35). Furthermore, the distribution of  $G^*$  narrows as the frequency increases (35). Phenomenological models to explain such a log-normal

distribution and/or a frequency-dependent distribution have been proposed (23,36), but the source of the observed cell-to-cell variation remains poorly understood.

To address these questions, we investigated the ensemble distribution of  $G^*$  versus frequency  $f$  using atomic force microscopy (AFM)-enabled loading of individual mouse fibroblast cells arranged on a microarray substrate (35,37). Actin filament structures were found to play a strong role in changing the frequency dependence of the ensemble distribution of  $G^*$ . Moreover, the standard deviation of the log-normal distribution varied depending on the measurement location on the cells. We discuss the inherent cell-to-cell variation of the cell samples observed by AFM, in terms of power-law rheology.

## MATERIALS AND METHODS

### Cell samples

Mouse fibroblast NIH3T3 cells (ATCC, Manassas, VA) were cultured at 37°C and 5% CO<sub>2</sub> atmosphere for 1–2 days in Dulbecco's modified Eagle's medium DMEM (Sigma-Aldrich, St. Louis, MO) containing penicillin (100 units/mL), streptomycin (100 mg/mL) (Sigma-Aldrich), and 10% fetal bovine serum (FBS; HyClone, Logan, UT). After suspension with trypsin (Sigma-Aldrich), cells were deposited in microarray wells of a hexagonal shape and a width of 20  $\mu$ m (LiveCell Array; Nunc, Penfield, NY) that were first coated with fibronectin (BD Biosciences, San Jose, CA), in complete medium (DMEM containing FBS) and immediately incubated for 12 h under the same conditions as described previously. For AFM measurements, the medium was replaced with CO<sub>2</sub>-independent medium (Invitrogen, Carlsbad, CA). A fluorescence image of the nuclei of NIH3T3 cells observed with a confocal optical microscope (DIGITAL ECLIPSE C1; Nikon, Tokyo, Japan) is shown in Fig. 1 *a*. By staining nuclei with DAPI, we confirmed that the average nucleus diameter was 10.7  $\mu$ m

Submitted February 6, 2013, and accepted for publication July 12, 2013.

\*Correspondence: okajima@ist.hokudai.ac.jp

Editor: Jeffrey Fredberg.

© 2013 by the Biophysical Society  
0006-3495/13/09/1093/10 \$2.00



<http://dx.doi.org/10.1016/j.bpj.2013.07.035>

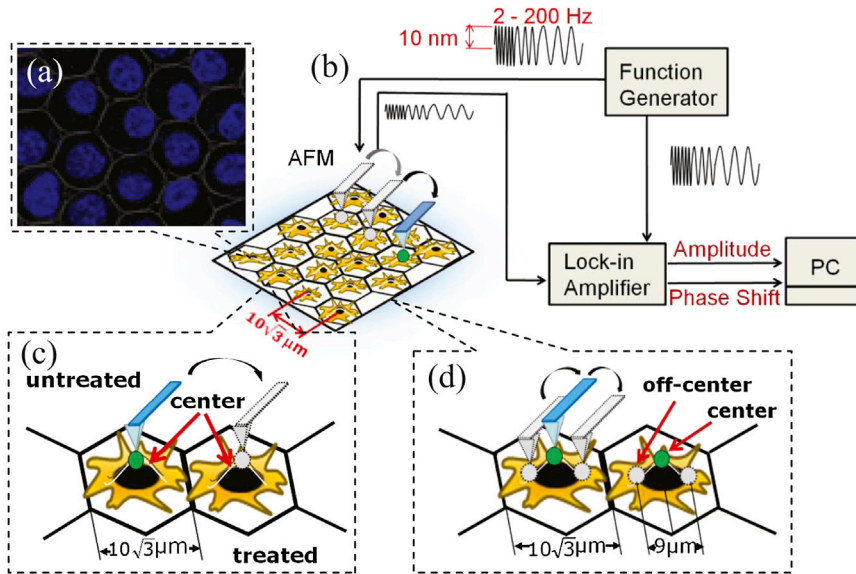


FIGURE 1 (a) Fluorescence image of nuclei of NIH3T3 cells deposited in microarray wells and cultured for 12 h using confocal microscopy. The cell nuclei were stained with DAPI. (b) Schematic of the AFM force modulation with a microarray substrate, on which living cells were arranged and cultured. (c) Measurements of the effect of cytoD on the  $G^*$  of cells. The untreated cells were measured at the center of wells and the same cells treated with cytoD were measured again at the same location. (d) Measurements of the spatial dependence of  $G^*$  of cells at different locations of the center and away from the center of wells.

and that the center of the nucleus fluctuated from the center of the well with a standard deviation of  $2.9 \mu\text{m}$  (see Fig. S1 in the Supporting Material).

## Measurements of cell rheology by AFM

A commercial AFM (MFP-3D AFM; Asylum Research, Santa Barbara, CA) mounted on an inverted optical microscope (TE-2000E; Nikon) was used to examine the rheology of NIH3T3 cells (Fig. 1 b). A rectangular cantilever (BioLever mini, BL-AC40TS-C2; Olympus, Tokyo, Japan) with a nominal spring constant of  $0.1 \text{ N/m}$  was used. To achieve a well-defined contact geometry, a colloidal silica bead with a radius  $R$  of  $\sim 2.5 \mu\text{m}$  (Funakoshi, Tokyo, Japan) was carefully attached to the apex of the AFM tip with epoxy (35,37,38). Before the cell experiments, the spring constant of the cantilever was determined in liquid environments using a built-in thermal fluctuation procedure. The loading force was determined using Hooke's law by multiplying the cantilever deflection by the calibrated cantilever spring constant.

For force modulation measurements, the cells in the wells were indented at an initial loading force of  $< 650 \text{ pN}$ . During indentation, the frequency of the modulation signal applied to a z-axis piezo actuator was not continuously swept but there was a stepwise change in frequency of  $f = 2, 5, 10, 25, 50, 100, \text{ and } 200 \text{ Hz}$ , with an amplitude of  $10 \text{ nm}$ . The duration of indentation for each frequency was typically  $3\text{--}7 \text{ s}$ . The amplitude and phase shift of the cantilever displacement with respect to the reference signal were measured using a digital lock-in amplifier (7260; SEIKO EG&G, Tokyo, Japan). To assure the stability of the lock-in amplifier, the averaging time became longer for lower frequencies. To measure a large number of cells (at least  $n = 80$ ) in a microarray sample, we limited the measurement time for each cell to be within  $1 \text{ min}$  and therefore the lowest frequency to be  $2 \text{ Hz}$ .

To investigate the effects of cytochalasin-D (cytoD) (Sigma-Aldrich), which inhibits actin filament polymerization, single cells were measured at the center of wells (essentially atop the nuclei), incubated in  $2 \mu\text{M}$  cytoD for  $20 \text{ min}$ , and measured again (Fig. 1 c). To investigate the spatial dependence of cell rheology parameters, measurements were performed at the center and  $4.5 \mu\text{m}$  from the center of wells for the same cells (Fig. 1 d). The off-center position was closer to the periphery of the cell nucleus but still within the nucleus boundaries for most cells (see Fig. S1).

According to the Hertzian contact model, the loading force  $F^*$ , which is complex as indicated by the asterisk, with a small amplitude indentation oscillation,  $\delta_1^*$  around an operating indentation,  $\delta_0$ , can be approximately expressed as (20,39–41)

$$F^* = \frac{4R^{1/2}}{3(1-\nu^2)} \left( E_0 \delta_0^{3/2} + \frac{3}{2} E_1^* \delta_0^{1/2} \delta_1^* \right), \quad (1)$$

where  $\nu$  is the Poisson's ratio of the cell, assumed here to be  $0.5$  (20), and  $E_0$  is the Young's modulus of the cell at zero frequency obtained from the slow-approach force-distance curve. The frequency-dependent Young's modulus  $E_1^*$  is given by  $2(1+\nu)G^*$  (42). While moving through a surrounding liquid, the probe is subject not only to the force applied to the cell, but also to a hydrodynamic drag force  $F_d^*$  given by  $F_d^*/\delta_1^* = ib(h)f$  (20,43), where  $b(h)$  is a viscous drag factor that depends on the separation distance  $h$  between the cell surface and the probe (20,43). Thus,  $G^*$  is given by (20)

$$G^* = G' + iG'' = \frac{1-\nu}{4(R\delta_0)^{1/2}} \left[ \frac{F_1^*}{\delta_1^*} - ib(0)f \right], \quad (2)$$

where  $G'$  and  $G''$  represent the storage and loss moduli of the cell, respectively,  $i$  is the imaginary unit, and  $F_1^* = 2(R\delta_0)^{1/2} E_1^* \delta_1^* / (1-\nu^2)$ . The value of  $b(0)$  was determined by extrapolating values of  $b(h)$  measured at various separation distances at  $f = 100 \text{ Hz}$ . The amplitude and phase response of the instrument including mechanics and electronics whose resonance was higher than the frequencies applied to cells was calibrated at different frequencies using a stiff cantilever in contact with a clean glass coverslip in air, and cell measurements were corrected accordingly.

## Data analysis

AFM data were analyzed using the Igor Pro software (WaveMetrics, Lake Oswego, OR) with a built-in global fitting procedure.  $G'$  and  $G''$  as a function of  $f$  were fitted to the power-law structural damping model with additional Newtonian viscosity (15,16,34), which is given by

$$G^* = G_0 g(\alpha) \{1 + i\eta(\alpha)\} \left( \frac{f}{f_0} \right)^\alpha + i\mu f. \quad (3)$$

Here,  $\alpha$  is the power-law exponent and  $g(\alpha) = \Gamma(1-\alpha) \cos(\pi\alpha/2)$  where  $\Gamma$  denotes the gamma function.  $G_0$  is a scale factor of the modulus at a frequency scale factor  $f_0$ , which was arbitrarily set to  $1 \text{ Hz}$ . The hysteresivity  $\eta(\alpha)$  is equivalent to  $\tan(\pi\alpha/2)$ , and  $\mu$  is the Newtonian viscous damping coefficient.

The standard deviation  $\sigma_X$  of a quantity  $X$  is expressed by

$$\sigma_X = \left[ \frac{1}{n-1} \sum_{j=1}^n (X_j - \langle X \rangle)^2 \right]^{1/2}, \quad (4)$$

where  $n$  is the total number of data,  $X_j$  denotes the individual  $j$ th data, and  $\langle X \rangle$  is the arithmetic mean of  $X$ . Hereafter,  $\bar{Z}$  denotes the geometric mean of quantity  $Z$  with a log-normal distribution. Student's  $t$ -test was used to test for statistically significant differences in the parameters of the structural damping model, and Pearson's correlation coefficient was used to characterize the correlation between  $G^*$  values measured at different subcellular locations.

## RESULTS

### Influence of actin filaments

The stiffness of attached cells measured by AFM is strongly associated with the cytoskeletal actin network organization (30,31), which is spatially heterogeneous and changes over time. Therefore, we first measured  $G^*$  of cells after actin filament polymerization was disrupted by cytoD (2  $\mu$ M). Fig. 2 shows the ensemble distribution of  $G^*$  of the treated and untreated cells measured at the center of wells by AFM at different frequencies. We note four observations. First,  $G^*$  consistently exhibited a log-normal distribution. Second, the geometric mean of  $G^*$  shifted to higher values with increasing  $f$ . Third, the distribution of  $G'$  became narrower with  $f$ , and the distributions of  $G''$  were narrower than those of  $G'$ . These features are consistent with those observed in previous studies (15,16,21–26,35). Fourth, the

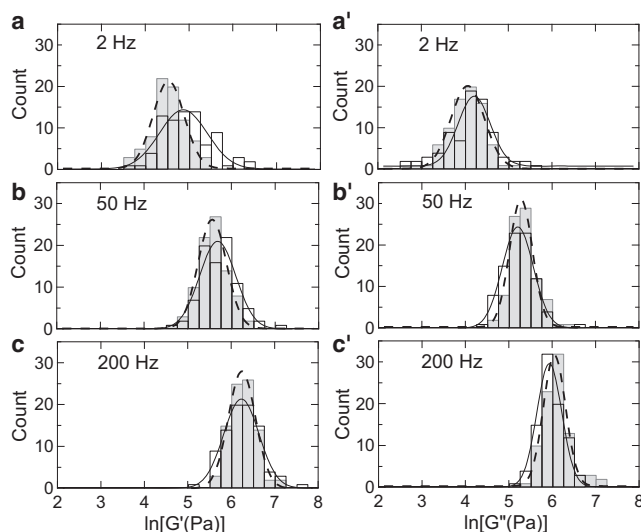


FIGURE 2 Distributions of the storage  $G'$  (left) and loss  $G''$  (right) moduli of untreated cells (white,  $n = 87$ ) and cytoD-treated cells (gray,  $n = 87$ ) in microarray wells at different frequencies: (a) 2, (b) 50, and (c) 200 Hz. The solid and dashed lines represent the fitted results of untreated and treated cells, respectively, using a log-normal distribution function.

distribution of  $G^*$  of the treated cells was narrower than that of the untreated cells.

To clarify the effect of cytoD on  $G^*$ , we plotted the ensemble average  $\bar{G}^*$  and the standard deviation of  $G^*$  distribution,  $\sigma_{\ln G^*}$ , versus frequency  $f$  (Fig. 3). As shown in Fig. 3,  $a$  and  $b$ ,  $\bar{G}^*$  increased with  $f$  and closely followed the structural damping equation (Eq. 3). The disruption of actin filament polymerization resulted in a decrease in  $\bar{G}_0$  by  $\sim 50\%$  ( $p < 10^{-5}$ ) and an increase in the average power-law exponent  $\langle \alpha \rangle$  from 0.32 to 0.37 ( $p < 10^{-5}$ ), which were similar behaviors to those reported in previous studies (15–18). As shown in Fig. 3  $a$ , the point at which the extrapolated lines of  $\bar{G}'$  for the treated and untreated cells intersect was defined as  $\bar{G}' = \bar{g}_0$  at  $f = \Phi_0$  (15,16).

Fig. 4 shows the ensemble distributions of the parameters of the power-law rheology of untreated and cytoD-treated cells, estimated from Eq. 3.  $G_0$  displayed a log-normal behavior with a distribution that was narrower after cytoD treatment. Measurements of the power-law exponent  $\alpha$  exhibited a Gaussian distribution that also became narrower after cytoD treatment, whereas  $\mu$  exhibited a log-normal distribution (see Fig. S2), and its mean value did not change significantly ( $p = 0.71$ ) after treatment. The standard deviations of these parameters are listed in Table 1.

The standard deviation of the complex modulus  $\sigma_{\ln G^*}$  was reduced in the treated cells (Fig. 3,  $c$  and  $d$ ), and the reduction was larger than that expected from the change in  $\ln \bar{G}^*$  (see Fig. S3). Moreover,  $\sigma_{\ln G^*}$  of the treated cells was smaller than that of the untreated cells when both  $\sigma_{\ln G^*}$  values were evaluated at the same  $\bar{G}^*$  values but different frequencies (see Fig. S4,  $a$  and  $b$ ). The results indicate a strong coupling between cell-to-cell variation and the cytoskeletal actin organization of cells.

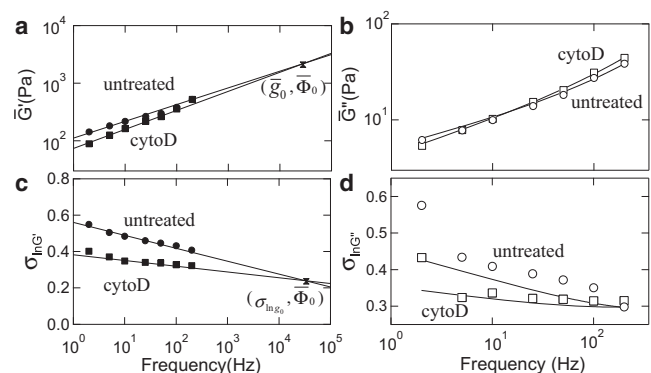


FIGURE 3 Frequency dependences of  $\bar{G}^*$  ( $\bar{G}'$  (a) and  $\bar{G}''$  (b)) of untreated (circle) and treated (square) cells. Solid lines in (a) and (b) represent the fitted results to Eq. 3. The mean squared error is 25.8 (a). The point where the curves of  $\bar{G}'$  intersect is defined as  $\bar{G}' = \bar{g}_0$  at  $f = \Phi_0$ . Frequency dependency of  $\sigma_{\ln G'}$  (c) and  $\sigma_{\ln G''}$  (d) of untreated (circle) and treated (square) cells. Solid lines in (c) and (d) represent the fitted results using Eqs. 7 and S19, respectively (see Discussion). The mean squared error is 0.011 (c).

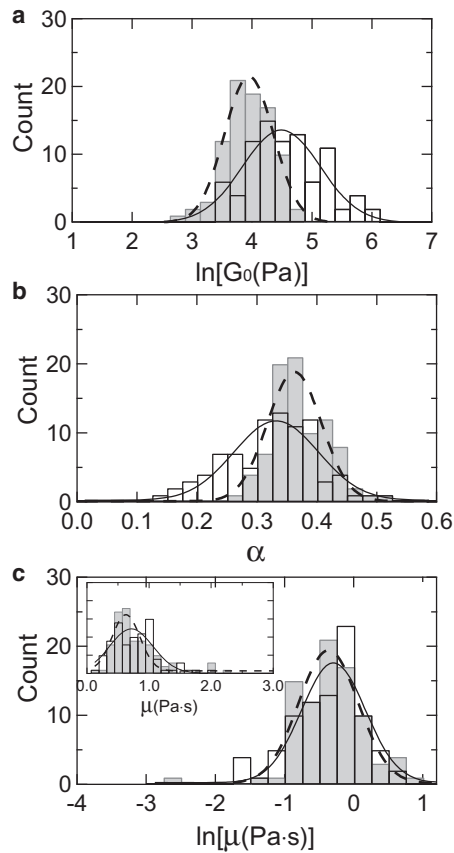


FIGURE 4 Distributions of (a)  $G_0$  on a logarithmic scale, (b)  $\alpha$  on a linear scale, and (c)  $\mu$  on a logarithmic scale of untreated (white) and treated (gray) cells. Inset in (c) shows the distribution of  $\mu$  on a linear scale. Solid and dashed lines represent the fitted results of untreated and treated cells, respectively, using a log-normal distribution function (a and c) and to a normal distribution function (b and inset in c).

### Spatial dependence

We next conducted AFM measurements to characterize the ensemble distribution of cell rheology parameters at two different locations on the cells: the center and 4.5  $\mu\text{m}$  away from the center of each microarray well. Measurement at both locations enables a comparison of mechanical response directly atop the cell nuclei with that measured toward the nuclear perimeter (see Methods). Fig. 5 shows the distribution of  $G^*$  for these two subcellular locations (center and off-center) at different frequencies. These distributions featured the same characteristic features as those observed in untreated and treated cells (see Fig. 2).

To quantify the distributions of  $G^*$ , we plot  $\bar{G}^*$  and  $\sigma_{\ln G^*}$  as a function of  $f$  in Fig. 6. The  $\bar{G}^*$  values, which fit well to the model described in Eq. 3 (Fig. 6, a and b), did not differ considerably between center and off-center locations. However, for all frequencies considered, the distribution of  $G^*$  measured at off-center locations was remarkably narrower than that measured at the well center (Fig. 6, c

**TABLE 1** Power-law rheological parameters obtained from a comparison of 1), untreated and cytoD-treated cells and 2), cells measured at the center and away from the center of microarray wells

	Center		Untreated	
	Untreated ( $n = 87$ )	cytoD ( $n = 87$ )	Center ( $n = 160$ )	Off-center ( $n = 160$ )
$\bar{G}_0$ (Pa) <sup>a</sup>	95.58	51.41	54.60	66.02
$\langle\alpha\rangle^a$	0.32	0.37	0.29	0.28
$\mu$ (Pa·s) <sup>a</sup>	0.75	0.70	0.62	0.64
$\sigma_{\ln G_0}^a$	0.62	0.41	0.82	0.72
$\sigma_\alpha^a$	0.08	0.05	0.09	0.08
$\sigma_{\ln \mu}^a$	0.65	0.61	0.59	0.41
$\Phi_0$ (Hz) <sup>b,c</sup>	$3.20 \times 10^4$	$3.20 \times 10^4$	$1.12 \times 10^4$	$1.12 \times 10^4$
$\sigma_{\ln \Phi_0}^c$	$0.24^{0.03}$	$0.24^{0.03}$	$0.38^{0.08}$	$0.38^{0.08}$
$\sigma_\alpha^c$	$0.031^{0.002}$	$0.014^{0.002}$	$0.042^{0.003}$	$0.029^{0.003}$
$\sigma_{\ln \mu}^c$	$0.35^{0.12}$	$0.37^{0.08}$	$0.62^{0.04}$	$0.44^{0.04}$

<sup>a</sup>Represents estimates using Eq. 4.

<sup>b</sup>Represents estimates from the plot of  $\ln G'$  vs.  $\ln f$ .

<sup>c</sup>Represents estimates from the plot of  $\sigma_{\ln G'}$  vs.  $\ln f$ .

and d). Indeed, plotting  $\sigma_{\ln G^*}$  vs.  $\ln \bar{G}^*$  showed that  $\sigma_{\ln G^*}$  for cells measured at the off-center location was smaller than that at the center for the same  $\bar{G}^*$  values (see Fig. S4, c and d). These results suggest that differences in rheological response among individual cells are reduced when mechanical loading occurs at locations beyond the cell center.

Fig. 7 shows the ensemble distributions of the parameters of the power-law rheology of cells, estimated from Eq. 3, at different subcellular locations. The shape of the distributions was unchanged, regardless of cell location;

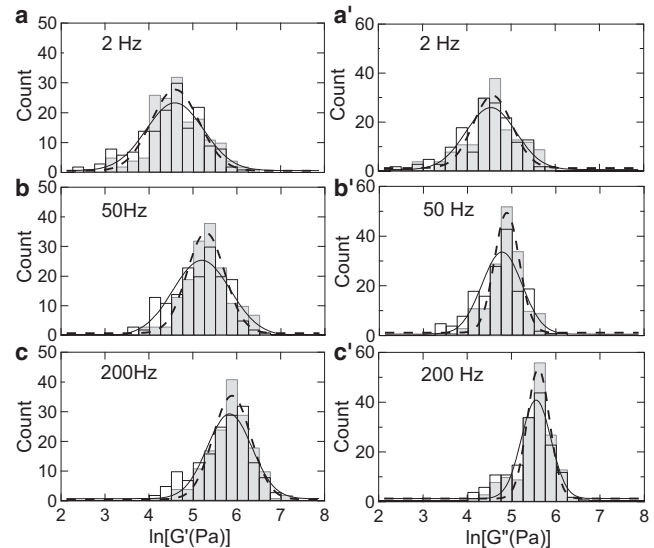


FIGURE 5 Distributions of  $G'$  (left) and  $G''$  (right) moduli of cells measured at center (white,  $n = 160$ ) and off-center (gray,  $n = 160$ ) locations of microarray wells at different frequencies: (a) 2, (b) 50, and (c) 200 Hz. Solid and dashed lines represent fitted results of cells measured at center and off-center locations, respectively, using a log-normal distribution function.



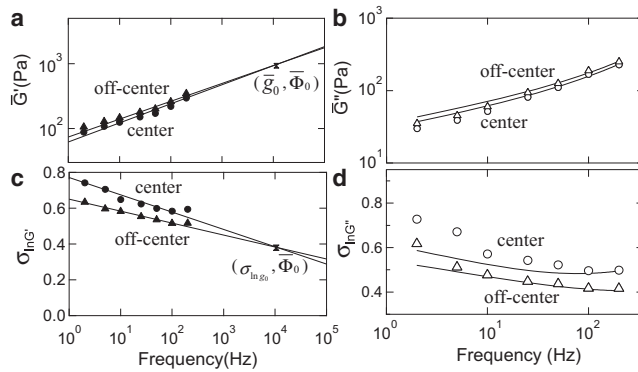


FIGURE 6 Frequency dependences of  $\bar{G}^*$  ( $\bar{G}'$ ) (a) and  $\bar{G}''$  (b) of cells measured at center (circle) and off-center (triangle) locations of wells. Solid lines in (a) and (b) represent the fitted results to Eq. 3. The mean squared error is 13.0 (a). The point where the curves of  $\bar{G}'$  intersect is defined as  $\bar{G}' = \bar{g}_0$  at  $f = \bar{\Phi}_0$ . Frequency dependences of  $\sigma_{\ln G^*}$  (c) and  $\sigma_{\ln G'}$  (d) of cells measured at center (circle) and off-center (triangle) locations of wells. Solid lines in (c) and (d) represent the fitted results using Eqs. 7 and S19, respectively (see Discussion). The mean squared error is 0.014 (c).

that is,  $G_0$  and  $\mu$  displayed a log-normal distribution, whereas  $\alpha$  exhibited a Gaussian distribution. Moreover, on every distribution of  $\ln G_0$ ,  $\alpha$ , and  $\ln \mu$ , the standard deviation measured at the center of wells was broader when compared with the corresponding value off-center (Table 1). Measurements of  $\ln G_0$  were different between cells measured at the center and away from the center of wells ( $p = 0.026$ ), consistent with previous reports (30,31,33,44), which showed that cell stiffness measured near the nucleus was relatively low and gradually increased toward the peripheral regions. Conversely, we found no such obvious difference for  $\ln \mu$  ( $p = 0.17$ ) or  $\alpha$  ( $p = 0.042$ ). The results imply that cells have a similar fluidity, intermediate between elastic solids and viscous liquids (10–13), even in different subcellular locations within the nucleus boundaries.

Fig. 8 shows the relation between  $G^*$  of cells measured at the center and away from the center of wells at different frequencies by replotting the data shown in Fig. 5. It was found that  $G^*$  of the cells measured at the center of wells were proportional to the corresponding magnitudes at the off-center, indicating that this intracellular rheological parameter, measured at different subcellular locations, is spatially correlated.

## DISCUSSION

### Power-law rheology models

It has been commonly recognized that  $G'$  exhibits single power-law behavior in the range of  $10^0$ – $10^2$  Hz. On the other hand,  $G'$  in other frequency ranges is still controversial, and there are different types of power-law rheology models that have been proposed, i.e., single (15,16) and multiple (26,29)

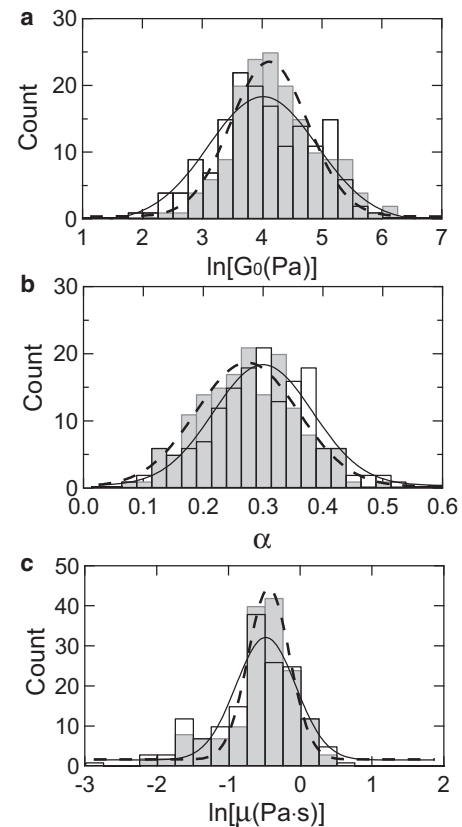


FIGURE 7 Distributions of (a)  $\ln G_0$ , (b)  $\alpha$  and (c)  $\ln \mu$  of cells measured at center (white) and off-center (gray) locations of wells. Solid and dashed lines represent the fitted results of cells measured at center and off-center locations, respectively, using a log-normal distribution function (a and c) and a normal distribution function (b).

power-law rheology models. Fabry et al. (15,16) reported that regardless of the treatments applied to cells,  $\bar{G}'$  of the cells as a function of  $f$  followed single power-law function in the frequency region of  $10^{-2}$ – $10^3$  Hz and appeared to cross at  $\bar{G}' = \bar{g}_0$  at a high frequency  $f = \bar{\Phi}_0$ . The behaviors have been observed in various types of cells and in different measurement techniques (15–17,45).

On the other hand, some studies reported multiple power-law behaviors of single cell rheology with two power-law exponents, which crossover at around  $10^0$  or  $10^2$  Hz. In the former case, the exponent in the lower frequency was beyond 0.5, which was considered to result from noncovalent protein-protein bond rupture during the near-equilibrium loading (29), whereas in the latter case, the exponent in the higher frequency was  $\sim 3/4$ , which was considered to probably arise from entropic fluctuations of a semiflexible-filament regime, and a soft-glass-like dynamics (26). In the intermediate frequency of  $10^0$ – $10^2$  Hz, the exponent was similar to that observed as single power-law rheology (15,16).

Here, we do not discuss the validity of cell rheology models from our present results because  $\bar{G}'$  was measured

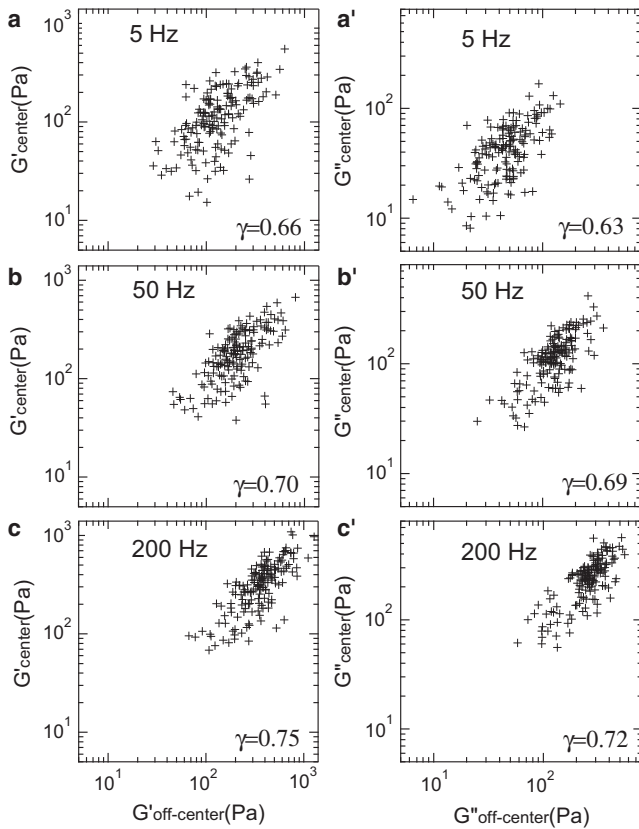


FIGURE 8  $G'$  measured at the center of wells,  $G'_{\text{center}}$ , vs.  $G'$  measured away from the center of wells,  $G'_{\text{off-center}}$  (left) and  $G''$  measured at the center of wells,  $G''_{\text{center}}$ , vs.  $G''$  measured away from the center of wells,  $G''_{\text{off-center}}$  (right), at different frequencies: (a) 5, (b) 50, and (c) 200 Hz. The data are the same as those shown in Figs. 5–7.

in only two decades of frequency range, i.e.,  $10^0$ – $10^2$  Hz. Nevertheless, as shown below, we found that the single power-law rheology model, which has the smallest number of fitting (rheological) parameters in power-law rheology models mentioned previously, allowed us to explain the frequency dependence of  $\sigma_{\ln G'}$  and to quantify the cell-to-cell variation, which was invariant in different cell samples prepared under the same conditions.

### Standard deviation of $\ln G'$

A crucial problem to estimate the cell-to-cell variation from the experimental results is that the magnitude of  $\sigma_{\ln G'}$  is largely varied in different sets of experiments. Namely, the magnitude of  $\sigma_{\ln G'}$  is quite different for two different pairs of conditions (Fig. 3 showing the effects of cytoD, and Fig. 6 showing the effects of subcellular measurement location), even though the control conditions in both sets of experiments (untreated, in the well center) were ostensibly identical. This suggests that the parameter  $\sigma_{\ln G'}$  observed experimentally in Figs. 3 c and 6 c, is not an exact invariant quantity, and can vary with challenges to the cell.

Therefore, we concluded that  $\sigma_{\ln G'}$  obtained in the present AFM study contains experimental variation such as instrumental noise and day-to-day influences under in vitro culture that we cannot control and explain.

To quantify the cell-to-cell variation in different sets of experiments under the same conditions, we derive the relationship among fitting parameters of the single power-law rheology model. We express  $G'$  for each cell as

$$G' = g_0 \left( \frac{f}{\Phi_0} \right)^\alpha, \quad (5)$$

where  $\Phi_0$  of each cell can be estimated by extrapolating the  $G'$  vs.  $f$  curves measured under one pair of two conditions. Both sets of data, plotted on a log-log scale, form lines that intersect at a point specified by  $(g_0, \Phi_0)$  that varies considerably (see Fig. S5), showing that cells exhibit global mechanical variation that can be conceptualized to correspond to the variation in depth of the potential energy well that a cytoskeletal element must overcome to escape the glass transition, according to soft glassy rheology (SGR) (10–12). Averaged over all cells, we obtain  $\bar{g}_0$  and  $\bar{\Phi}_0$  (Table 1).

The linear relation between  $\ln G_0$  and  $\alpha$  for each cell is then given by (see Eq. S6)

$$\ln G_0 = \ln \bar{g}_0 - \left[ \ln \left( \frac{\bar{\Phi}_0}{f_0} \right) + \frac{d \ln g(\alpha)}{d\alpha} \right] \alpha, \quad (6)$$

where  $\ln g(\alpha)$  is reasonably assumed to be approximately linear to  $\alpha$  (see Fig. S6 a). In Fig. 9 a, we replot  $\ln G_0$  vs.  $\alpha$ , measured at the center and off-center locations of wells,

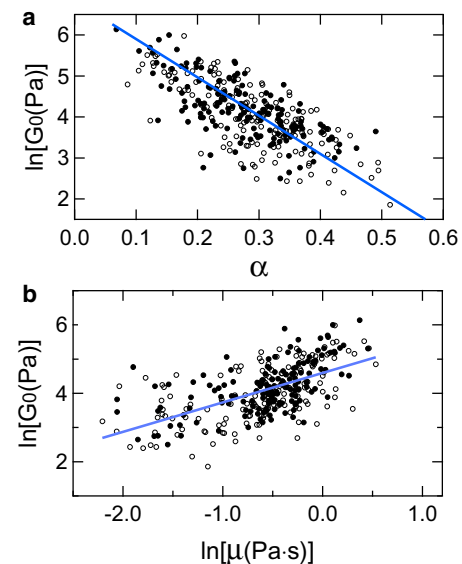


FIGURE 9 Plots of  $\ln G_0$  vs.  $\alpha$  (a) and  $\ln G_0$  vs.  $\ln \mu$  (b) of cells measured at center (open circle) and off-center (solid circle) locations of cells, which are shown in Figs. 5–7. The solid lines in (a) and (b) represents the fitted results using Eq. 6 and a linear function, respectively.

which are presented in Figs. 5–7. The result fits well to Eq. 6 with  $\bar{g}_0$  and  $\bar{\Phi}_0$ . Moreover, the plot of  $\ln G_0$  vs.  $\ln \mu$  suggests a linear relationship (Fig. 9 b).

Thus, we can express  $\sigma_{\ln G'}$  of cells from Eq. 3 as (see Eq. S15)

$$\sigma_{\ln G'} = \sigma_{\ln g_0} + (\ln \bar{\Phi}_0 - \ln f) \sigma_\alpha, \quad (7)$$

showing that  $\sigma_{\ln G'}$  is proportional to  $\ln f$  with a slope of  $-\sigma_\alpha$  at  $f < \bar{\Phi}_0$  (36), and that the variation, from all sources, in these cells' mechanical response is characterized by  $\sigma_{\ln g_0}$  at  $f = \bar{\Phi}_0$ . Interestingly, we fit  $\sigma_{\ln G'}$  shown in Figs. 3 and 6 to Eq. 7 and found that the curves of  $\sigma_{\ln G'}$  under one pair of two conditions can be crossed at the point  $(\sigma_{\ln g_0}, \bar{\Phi}_0)$  (Table 1).

Fig. 10 shows  $\tilde{\sigma}_{\ln G'}$ , which is defined as  $\sigma_{\ln G'} - \sigma_{\ln g_0}$ , as a function of  $f$  estimated from Figs. 3 c and 6 c. Importantly, the values of  $\tilde{\sigma}_{\ln G'}$  for cells from control conditions in different experiments (i.e., untreated and measured at the center of wells in each experimental pairwise comparison) were similar even in different pairs of experimental conditions (e.g., control conditions in Figs. 3 and 6). Moreover, it was found that the features of  $\tilde{\sigma}_{\ln G'}$  with  $f$  remained even after the definition of the standard deviation was changed from  $\sigma_{\ln G'}$  to  $\tilde{\sigma}_{\ln G'}$ , i.e., 1),  $\tilde{\sigma}_{\ln G'}$  of cells treated with cytoD was largely reduced compared with that of the control cells (see Fig. S3 c); and 2),  $\tilde{\sigma}_{\ln G'}$  away from the center of wells was smaller than the corresponding value at the center. Therefore, the frequency dependence of  $\tilde{\sigma}_{\ln G'}$  apparently varies with the integrity of the actin network, and the cell-to-cell mechanical variation exhibits a spatial dependence. The inherent cell-to-cell variation of  $G'$  in the frequency domain was schematically shown in Fig. 11.

The parameter  $\sigma_{\ln G''}$  could not be analytically solved based on the single power-law rheology model, and thus a first-order approximate formula of  $\sigma_{\ln G''}$  was derived from Eq. 3 (details of deriving the formula of  $\sigma_{\ln G''}$  are given in

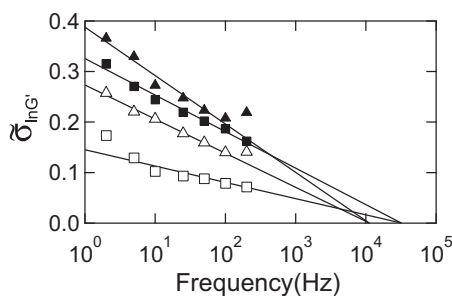


FIGURE 10  $\tilde{\sigma}_{\ln G'}$ , which represents  $\sigma_{\ln G'} - \sigma_{\ln g_0}$  as a function of  $\ln f$ . The results obtained from two cell samples shown in Fig. 3 c and in Fig. 6 c are replotted: One sample is untreated (solid rectangle) and treated (open rectangle) cells measured at the center of wells, whereas the other is untreated cells measured at the center (solid triangle) and away from the center (open triangle) of wells. Solid lines represent the fitted results using Eq. 7.

Eq. S19). We can see in Figs. 3 d and 6 d that Eq. S19 is semiquantitatively valid for the observed  $\sigma_{\ln G''}$ ; however, Eq. S19 remains only an approximation for this parameter.

### Standard deviation of $\alpha$

We observed that the  $\sigma_\alpha$  values estimated from the slope of  $\sigma_{\ln G'}$  in Figs. 3 c and 6 c was smaller than those obtained from the distribution of  $\alpha$  shown in Figs. 4 b and 7 b (Table 1). This finding suggested that  $\sigma_\alpha$ 's estimated from the frequency dependence of  $G^*$  in each cell group with Eq. 3 contain a substantial fitting error in addition to the inherent cell-to-cell variation.

It is noted that  $\sigma_{\ln G'}$  values measured under one pair of two conditions were different even at the same value of  $\bar{G}'$  (see Fig. S4), suggesting that the  $\sigma_{\ln G'}$  value is not simply governed by the magnitude of  $\bar{G}'$ . The  $\sigma_{\ln G'}$  as a function of  $\ln \bar{G}'$  (Eq. S21) is also expressed as

$$\sigma_{\ln G'} = \sigma_{\ln g_0} + \frac{\sigma_\alpha}{\langle \alpha \rangle} (\ln \bar{g}_0 - \ln \bar{G}'), \quad (8)$$

showing that  $\sigma_{\ln G'}$  decreases with increasing  $\ln \bar{G}'$  with a slope of  $\sigma_\alpha / \langle \alpha \rangle$ . The value of  $\sigma_\alpha / \langle \alpha \rangle$  was 0.11 and 0.035 for the untreated and treated cells, respectively, although it is 0.15 and 0.11 for cells measured at center and off-center locations of the wells, respectively (Table 1). Using these values, we found that the plots of  $\sigma_{\ln G'}$  vs.  $\ln \bar{G}'$  fit well to Eq. 8 (see Fig. S4, a and c). Therefore,  $\sigma_\alpha / \langle \alpha \rangle$  is interpreted as a measure of the variation in mechanical response of cell groups with the same  $\ln \bar{G}'$  measured in different conditions.

In SGR, the power-law exponent of  $G'$  is related to the transition probability between the potential wells, i.e., the transition rate decreases with decreasing the exponent (10–12). In the molecular points of view, the SGR elements and the energy wells can be identified with myosin motors and the binding energies between myosin and actin, respectively (12). This model suggests that the depolymerization of actin filaments by cytoD leads the reduction of the actin-myosin interactions and the enhancement of the spatial homogeneity of the interactions.

### Sources of experimental uncertainty

It is noted that there are still at least three main sources of experimental uncertainty in this study. The first is the imperfection of cell sample preparation, in which the cells are not perfectly centered within each well, so the exact location of the nucleus center and perimeter vary correspondingly. To understand how such cell preparations influence the observed distribution of  $G'$ , let us assume an ideal condition in which the subcellular mechanical heterogeneity of each cell measured by AFM is identical and fixed according to Fig. 11. When these identical cells are deposited with



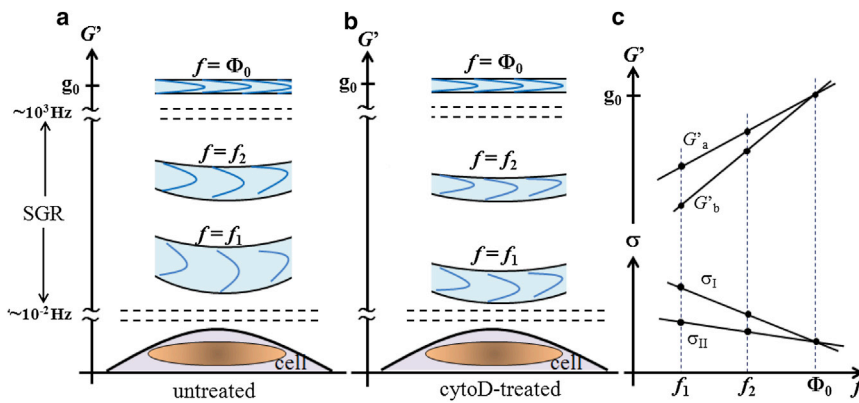


FIGURE 11 Schematic of  $G'$  of untreated cells (a) and cytoD-treated cells (b) at different frequencies. The cell-to-cell variation of  $G'$  varies depending on intracellular locations: the distribution narrows when changing from cell center to cell nucleus boundaries. The spatial component of cell-to-cell variation of  $G'$  between the untreated and treated cells decreases with increasing  $f$ , and consequently both cells become spatially homogeneous at  $f = \Phi_0$  beyond the SGR region (see Eq. 7), but the cell-to-cell variation still exists at  $f = \Phi_0$ . The spatial variation of  $G'$  for the untreated cells in the SGR region is larger than that for treated cells. One experimental condition is that  $G'_a(\sigma_{II})$  and  $G'_b(\sigma_I)$  represent the values measured at off-center and center locations, respectively, whereas the other  $G'_a(\sigma_I)$  and  $G'_b(\sigma_{II})$  are those of the untreated and treated cells, respectively (c).

randomized locations of the cell center within the microarray wells, we must inevitably observe a distribution of  $G^*$  of cells in which variation arises due to the fluctuation of cell positions in the wells. It is noted that the distribution in  $G'$  for cells measured at the center is relatively large compared with corresponding distribution in  $G'$  away from the center because the spatial heterogeneities within cells increase toward the cell center (Fig. 11 a). Moreover, the distribution width is reduced when cells are treated with cytoD because the spatial heterogeneity of treated cells is smaller than that of untreated ones (Fig. 11 b).

The second is the cell-cell contact of the cell sample. Cells on microwells have almost the same size and shape, which allows us to compare measurements at the same position between different cells, and to blindly touch down the AFM tip and still know exactly where we have probed the cell. This tremendously speeds up the measurements as we no longer need to visually search for cells. On the other hand, cells in our microarrays form cell-cell contacts on all six intersecting sides, and therefore we expect the cells to have both physical and chemical interactions, and furthermore we expect that these contacts influence cell-mechanical properties and their distributions (compared with isolated nonconfluent cells). It has been reported in a previous study (29) on human airway smooth muscle cells that cell-cell contacts play only a minor role. However, in most other studies of single cell rheology, cell-cell contacts are usually not well controlled or characterized, and thus the relationship between single cell rheology and cell rheology in a sheet of cells is not well understood.

The third is related to the AFM experimental method, in which the AFM probe indents the cells by applying an initial force. This causes a change in the indentation depth among cells measured by AFM because the depth depends on the cell stiffness. It is known that the AFM is capable of detecting the mechanical properties of highly tensed deep cytoskeleton such as stress fibers, rather than the flexible

cortical cytoskeleton (30,31). Rheological measurements of cells depend to some degree on the complex modulus as a function of cell depth, which is not identical among the measured cells.

### Variation in measured rheological properties of cells

Several techniques have been employed to measure the rheological properties of single cells. Previous studies have revealed that the value of  $\alpha$  was in the range of 0.1–0.4, regardless of the techniques employed (10–13). The results presented in Fig. 6 are in agreement with these previous results in which  $\alpha$  is relatively insensitive to the subcellular measurement position. On the other hand, the mean  $G_0$  value was dependent on the measurement position (Table 1). It has been reported that cell stiffness—as measured by AFM in terms of the apparent Young's modulus, which is related to  $G_0$  (see Fig. S8)—is a useful indicator to distinguish normal and abnormal cells (46,47). Our results suggest that the precise control of the measurement position of cells is crucial to obtain clear correlations between the rheological properties and biological states of adherent cells.

### CONCLUSIONS

The cell-to-cell variation in rheological parameters measured via AFM oscillatory loading was quantified as a standard deviation,  $\tilde{\sigma}_{\ln G'}$ , in which the contribution of the variation at a crossover frequency  $f = \Phi_0$  containing experimental variation was subtracted from the variation measured by AFM. We found that  $\tilde{\sigma}_{\ln G'}$  observed for different cell populations under the same conditions was almost identical. The value of  $\tilde{\sigma}_{\ln G'}$  of cells treated with cytoD was significantly reduced, indicating that  $\tilde{\sigma}_{\ln G'}$  can be varied by perturbing the cytoskeleton at least via altered actin polymerization. Moreover,  $\tilde{\sigma}_{\ln G'}$  measured at the

center of microarray wells containing single cells was larger than that measured within the cell nucleus boundaries away from the well centers, suggesting that cell-to-cell variation of  $G'$  also exhibits a subcellular spatial dependence related to cytoskeletal organization.

## SUPPORTING MATERIAL

Eight figures, twenty-one equations, and supporting analysis are available at [http://www.biophysj.org/biophysj/supplemental/S0006-3495\(13\)00857-6](http://www.biophysj.org/biophysj/supplemental/S0006-3495(13)00857-6).

This work was supported by the Industrial Technology Research Grant Program (06A26007a) from the New Energy and Industrial Technology Development Organization (NEDO) of Japan (T.O.), Grant-in-Aids for challenging Exploratory Research (23656055) and for Scientific Research on Innovative Areas "Bio-assembler" (24106501) from the Japan Society for the Promotion of Science (T.O.), the Global-COE Program from the Ministry of Education, Culture, Sports, Science and Technology of Japan (T.O.), National Research Foundation Singapore through the Singapore-MIT Alliance for Research and Technology's BioSystems & Micromechanics IRG research programme (K.J.V.V. and J.M.M.), NSF CAREER CBET-0644846 (K.J.V.V.), and the NIH/NIBIB Molecular, Cellular, Tissue and Biomechanics Training Grant EB006348 (J.M.M.).

## REFERENCES

- Schmidt, C. E., A. F. Horwitz, ..., M. P. Sheetz. 1993. Integrin-cytoskeletal interactions in migrating fibroblasts are dynamic, asymmetric, and regulated. *J. Cell Biol.* 123:977–991.
- Bursac, P., G. Lenormand, ..., J. J. Fredberg. 2005. Cytoskeletal remodelling and slow dynamics in the living cell. *Nat. Mater.* 4:557–561.
- Kasza, K. E., A. C. Rowat, ..., D. A. Weitz. 2007. The cell as a material. *Curr. Opin. Cell Biol.* 19:101–107.
- Fletcher, D. A., and R. D. Mullins. 2010. Cell mechanics and the cytoskeleton. *Nature.* 463:485–492.
- Ingber, D. E. 2003. Tensegrity I. Cell structure and hierarchical systems biology. *J. Cell Sci.* 116:1157–1173.
- Discher, D. E., P. Janmey, and Y. L. Wang. 2005. Tissue cells feel and respond to the stiffness of their substrate. *Science.* 310:1139–1143.
- Janmey, P. A., and C. A. McCulloch. 2007. Cell mechanics: integrating cell responses to mechanical stimuli. *Annu. Rev. Biomed. Eng.* 9:1–34.
- Janmey, P. A., and D. A. Weitz. 2004. Dealing with mechanics: mechanisms of force transduction in cells. *Trends Biochem. Sci.* 29:364–370.
- Vogel, V., and M. Sheetz. 2006. Local force and geometry sensing regulate cell functions. *Nat. Rev. Mol. Cell Biol.* 7:265–275.
- Trepat, X., G. Lenormand, and J. J. Fredberg. 2008. Universality in cell mechanics. *Soft Matter.* 4:1750–1759.
- Kollmannsberger, P., and B. Fabry. 2009. Active soft glassy rheology of adherent cells. *Soft Matter.* 5:1771–1774.
- Kollmannsberger, P., and B. Fabry. 2011. Linear and nonlinear rheology of living cells. *Annu. Rev. Mater. Res.* 41:75–97.
- Hoffman, B. D., and J. C. Crocker. 2009. Cell mechanics: dissecting the physical responses of cells to force. *Annu. Rev. Biomed. Eng.* 11:259–288.
- Yamada, S., D. Wirtz, and S. C. Kuo. 2000. Mechanics of living cells measured by laser tracking microrheology. *Biophys. J.* 78:1736–1747.
- Fabry, B., G. N. Maksym, ..., J. J. Fredberg. 2001. Scaling the microrheology of living cells. *Phys. Rev. Lett.* 87:148102-1–148102-4.
- Fabry, B., G. N. Maksym, ..., J. J. Fredberg. 2003. Time scale and other invariants of integrative mechanical behavior in living cells. *Phys. Rev. E Stat. Nonlin. Soft Matter Phys.* 68:041914.
- Puig-de-Morales, M., E. Millet, ..., J. J. Fredberg. 2004. Cytoskeletal mechanics in adherent human airway smooth muscle cells: probe specificity and scaling of protein-protein dynamics. *Am. J. Physiol. Cell Physiol.* 287:C643–C654.
- Laudadio, R. E., E. J. Millet, ..., J. J. Fredberg. 2005. Rat airway smooth muscle cell during actin modulation: rheology and glassy dynamics. *Am. J. Physiol. Cell Physiol.* 289:C1388–C1395.
- Dahl, K. N., A. J. Engler, ..., D. E. Discher. 2005. Power-law rheology of isolated nuclei with deformation mapping of nuclear substructures. *Biophys. J.* 89:2855–2864.
- Alcaraz, J., L. Buscemi, ..., D. Navajas. 2003. Microrheology of human lung epithelial cells measured by atomic force microscopy. *Biophys. J.* 84:2071–2079.
- Hoffman, B. D., G. Massiera, ..., J. C. Crocker. 2006. The consensus mechanics of cultured mammalian cells. *Proc. Natl. Acad. Sci. USA.* 103:10259–10264.
- Van Citters, K. M., B. D. Hoffman, ..., J. C. Crocker. 2006. The role of F-actin and myosin in epithelial cell rheology. *Biophys. J.* 91:3946–3956.
- Balland, M., N. Desprat, ..., F. Gallet. 2006. Power laws in microrheology experiments on living cells: comparative analysis and modeling. *Phys. Rev. E Stat. Nonlin. Soft Matter Phys.* 74:021911-1–021911-17.
- Massiera, G., K. M. Van Citters, ..., J. C. Crocker. 2007. Mechanics of single cells: rheology, time dependence, and fluctuations. *Biophys. J.* 93:3703–3713.
- Desprat, N., A. Richert, ..., A. Asnacios. 2005. Creep function of a single living cell. *Biophys. J.* 88:2224–2233.
- Deng, L. H., X. Trepat, ..., J. J. Fredberg. 2006. Fast and slow dynamics of the cytoskeleton. *Nat. Mater.* 5:636–640.
- Overby, D. R., B. D. Matthews, ..., D. E. Ingber. 2005. Novel dynamic rheological behavior of individual focal adhesions measured within single cells using electromagnetic pulling cytometry. *Acta Biomater.* 1:295–303.
- Stamenović, D., N. Rosenblatt, ..., D. E. Ingber. 2007. Rheological behavior of living cells is timescale-dependent. *Biophys. J.* 93:L39–L41.
- Chowdhury, F., S. Na, ..., N. Wang. 2008. Is cell rheology governed by nonequilibrium-to-equilibrium transition of noncovalent bonds? *Biophys. J.* 95:5719–5727.
- Rotsch, C., and M. Radmacher. 2000. Drug-induced changes of cytoskeletal structure and mechanics in fibroblasts: an atomic force microscopy study. *Biophys. J.* 78:520–535.
- Haga, H., S. Sasaki, ..., T. Sambongi. 2000. Elasticity mapping of living fibroblasts by AFM and immunofluorescence observation of the cytoskeleton. *Ultramicroscopy.* 82:253–258.
- Heidemann, S. R., and D. Wirtz. 2004. Towards a regional approach to cell mechanics. *Trends Cell Biol.* 14:160–166.
- Park, C. Y., D. Tambe, ..., J. J. Fredberg. 2010. Mapping the cytoskeletal prestress. *Am. J. Physiol. Cell Physiol.* 298:C1245–C1252.
- Fredberg, J. J., and D. Stamenovic. 1989. On the imperfect elasticity of lung tissue. *J. Appl. Physiol.* 67:2408–2419.
- Hiratsuka, S., Y. Mizutani, ..., T. Okajima. 2009. The number distribution of complex shear modulus of single cells measured by atomic force microscopy. *Ultramicroscopy.* 109:937–941.
- Maloney, J. M., and K. J. Van Vliet. 2011. On the origin and extent of mechanical variation among cells. arXiv:1104.0702v2.
- Mizutani, Y., M. Tsuchiya, ..., T. Okajima. 2008. Elasticity of living cells on a microarray during the early stages of adhesion measured by atomic force microscopy. *Jpn. J. Appl. Phys.* 47:6177–6180.
- Ducker, W. A., T. J. Senden, and R. M. Pashley. 1991. Direct measurement of colloidal forces using an atomic force microscope. *Nature.* 353:239–241.
- Radmacher, M., R. W. Tillmann, ..., H. E. Gaub. 1992. From molecules to cells: imaging soft samples with the atomic force microscope. *Science.* 257:1900–1905.

40. Radmacher, M., R. W. Tillmann, and H. E. Gaub. 1993. Imaging viscoelasticity by force modulation with the atomic force microscope. *Biophys. J.* 64:735–742.
41. Mahaffy, R. E., S. Park, ..., C. K. Shih. 2004. Quantitative analysis of the viscoelastic properties of thin regions of fibroblasts using atomic force microscopy. *Biophys. J.* 86:1777–1793.
42. Landau, L., and E. M. Lifshitz. 1986. *Theory of Elasticity*. Pergamon Press, Oxford.
43. Alcaraz, J., L. Buscemi, ..., D. Navajas. 2002. Correction of microrheological measurements of soft samples with atomic force microscopy for the hydrodynamic drag on the cantilever. *Langmuir*. 18:716–721.
44. Nagayama, M., H. Haga, and K. Kawabata. 2001. Drastic change of local stiffness distribution correlating to cell migration in living fibroblasts. *Cell Motil. Cytoskeleton*. 50:173–179.
45. Djordjević, V. D., J. Jarić, ..., D. Stamenović. 2003. Fractional derivatives embody essential features of cell rheological behavior. *Ann. Biomed. Eng.* 31:692–699.
46. Lekka, M., P. Laidler, ..., A. Z. Hryniewicz. 1999. Elasticity of normal and cancerous human bladder cells studied by scanning force microscopy. *Eur. Biophys. J.* 28:312–316.
47. Cross, S. E., Y. S. Jin, ..., J. K. Gimzewski. 2007. Nanomechanical analysis of cells from cancer patients. *Nat. Nanotechnol.* 2:780–783.